Control Engineering Practice 142 (2024) 105766

Contents lists available at ScienceDirect

Control Engineering Practice

journal homepage: www.elsevier.com/locate/conengprac

A real-time capable method for planning minimum energy trajectories for one degree-of-freedom mechatronic systems

Domenico Dona' [a,*], Basilio Lenzo [a], Paolo Boscariol [b], Giulio Rosati [a]

[a] Dipartimento di Ingegneria Industriale (DII), Università degli Studi di Padova, Via Venezia 1, Padova, 31153, Italy
[b] Dipartimento di Tecnica e Gestione dei Sistemi Industriali (DTG), Università degli Studi di Padova, Stradella S. Nicola 3, Vicenza, 36100, Italy

ARTICLE INFO

Keywords:
Energy saving
Optimal control
Efficiency
Optimization
Servo-actuated system

ABSTRACT

The synthesis of optimal motion profiles has shown to be a successful and virtually inexpensive solution for enhancing energy efficiency of mechatronic systems. A typical application is the design of point-to-point motion profiles for one-degree-of-freedom mechatronic systems. This paper proposes a new method for designing minimum energy trajectories for servo-actuated systems. The problem is solved by exploiting the knowledge of the structure of the optimal solution. That allows to solve the motion design problem by solving a set of nonlinear equations and, if needed, some basic optimization procedures, formulated after some suitable continuity conditions.

The herein proposed method applies to systems with and without energy regeneration capability, for maximum adaptability to most industrial applications. The method also handles jerk, acceleration, and velocity constraints, which are typical requirements in many practical applications. The number of equations and thereby the computational time depends on the number of active constraints and on whether negative power is dissipated or regenerated. Overall, the method results to be suitable for Real-Time applications, also in the most challenging case in which all the constraints are active and the system cannot regenerate negative electric power. The accuracy and the effectiveness of the planning method is tested numerically, by comparing the solution to the one obtained by a general purpose optimal control solver and then also experimentally using a lab prototype.

1. Introduction

1.1. Motivation

CO_2 emission reduction is crucial to limit global warming and its consequences. According to Martins, Felgueiras, and Smitková (2018), about 60% of electricity in Europe comes from fossil fuels, while according to De Almeida, Fong, Brunner, Werle, and Van Werkhoven (2019) 53% of the worldwide electricity consumption in 2015 was due to electric motors, 60% of which in industry. Similar figures are reported also in the work (Saidur, 2010), while in Engelmann (2009) it is stated that as much as 8% of the energy required in production processes is used by robotic systems. This motivates research efforts aimed at reducing energy consumption in automatic machines and robots.

1.2. Existing approaches

Considering electric motor-driven applications, various solution have been proposed in the literature, which can be divided into two main groups: (a) hardware and (b) software solutions (Carabin, Wehrle, & Vidoni, 2017). The hardware ones are more challenging to implement since they require invasive, and sometimes costly, modifications to the system. Interesting examples are Hagn et al. (2008), Kim (2015) in which energy efficiency is ensured by using lighter parts. Another possibility is to add elastic elements to exploit efficient conversion between kinetic and potential energy (Bettega, Richiedei, Tamellin, & Trevisani, 2023; Palomba, Wehrle, Carabin, & Vidoni, 2020; Richiedei & Trevisani, 2020; Scalera, Carabin, Vidoni, & Wongratanaphisan, 2019). Efforts to minimize energy consumption were also directed towards hydraulic-actuated systems (Du, Plummer, & Johnston, 2017).

Software solutions have the advantage of an easier implementation. They can be applied to both single-axis systems and multi-axis manipulators. Point-To-Point (PTP) motions are a typical application. Referring to single-axis systems, several works have investigated the possibility of reducing energy expenditure (EE) of PTP motions. One possibility is to parameterize a motion profile using polynomials or piecewise polynomials, which can be then optimized by tuning a reduced set of

* Corresponding author.
E-mail address: domenico.dona@phd.unipd.it (D. Dona').

https://doi.org/10.1016/j.conengprac.2023.105766
Received 30 August 2023; Received in revised form 9 October 2023; Accepted 24 October 2023
Available online 16 November 2023

parameters. For example, in Assad et al. (2018) the parameters of an S-curve are tuned to minimize energy consumption using the Particle Swarm Optimization method. On the contrary in Tho, Kaneshige, and Terashima (2020) the parameter of a S-curve were tuned using mixed nonlinear-integer program for minimum time movement of a crane avoiding oscillation of the load . A similar problem was addressed in Yu, Han, and Haihua (2015) where the parameters of a trapezoidal law were determined with an optimization problem that was made convex through an appropriate parametrization. Polynomial functions were used in Huang, Hsu, and Fung (2011) to reduce the energy consumption of a motor-toggle servomechanism. Reinforcement Learning was used in Lin et al. (2023) for solving the minimum-energy problem with complex constraints. Even if these methods are simple to implement, they do not ensure the actual minimum energy consumption is achieved, as the solution is biased by the chosen basis function. In fact, the optimal trajectory may not be a polynomial. Optimal control solution methods are needed to find such a trajectory, such as Pontryagin's maximum principle (PMP).

The application of PMP can be found in several works, including Park (1996), Wang, Ueda, and Bortoff (2012, 2013), Wang, Zhao, Bortoff, and Ueda (2014). In Park (1996) trajectories that minimize the copper losses were derived assuming that the minimization of copper losses is equivalent to the minimization of the energy consumption. This assumption is however valid only if no mechanical losses are assumed, considering therefore the load as a purely conservative mechanical system, and taking into account only the availability of a motor drive that allows negative power regeneration. Both these assumptions are not considered to be valid in this work.

An interesting and complete discussion on the application of PMP for energy efficiency maximization for PTP motions has been conducted in Wang et al. (2013). The existence of the optimal solution is discussed for both the cases in which negative power is regenerated and dissipated. Acceleration and velocity constraints were introduced using the indirect adjoining approach, where state constraints are introduced augmenting the Hamiltonian. The junction conditions among sub-trajectories are derived using the Weierstrass–Erdmann conditions. The solution is found numerically using a multiple shooting method. However, the proposed solution is not suitable for on-line applications.

In Wang et al. (2014) an on-line solution is presented. Acceleration and velocity constraints are introduced using an iterative algorithm to find the junction points between consecutive arcs. However, only the special (and less challenging) case with negative power regeneration is addressed. In a more realistic scenario, negative power is dissipated in a resistor brake due to the lack of accumulators connected to the grid. As stated in Meike and Ribickis (2011), the use of accumulators in automatic systems has a large break-even point, making this solution seldom economically advantageous. The challenging aspect of considering negative power dissipation is handling the ensuing switch in the Hamiltonian (Ho et al., 2019), as will be explained in detail in Section 4.

Similar approaches have been applied to mobile-robot systems, where energy expenditure is of critical importance due to their reliance on battery power and the associated limited autonomy problem. When performing straight paths, the system dynamics is equivalent to a 1 DOF (Degree-Of-Freedom) system. The solution of the minimum-energy trajectories was studied in Kim and Kim (2007, 2013). Those applications coped with on-line requirements but no constraints on jerk/acceleration/velocity were considered. Moreover, the solution does not handle negative power dissipation because, in the specific application to mobile robots, negative power can be stored in the battery.

1.3. Contribution of this work

In light of the above, to the best of the authors' knowledge, there is no method that meets all of the following requirements: (i) use a variational solution for improved accuracy; (ii) can handle both negative power regeneration and negative power dissipation; (iii) can handle hard constraints on velocity, acceleration and jerk; (iv) is real-time capable. The proposed work therefore aims at filling this literature gap.

This paper presents a method to derive optimal (in terms of minimum energy consumption) trajectories for PTP motions. Jerk, acceleration, and velocity limits are considered. The method can deal with negative power regeneration and the less straightforward case in which negative power is dissipated. The method is Real-Time capable, as the time needed to compute an optimal motion profile, usually in the order of ms, is small compared to the time needed to actually perform the motion task, allowing therefore to plan the motion just before executing it without introducing a significant delay. Solving optimal control problems with hard constraints on controls and especially states is usually not trivial and requires efficient algorithms (Bryson & Ho, 2018). This is also true for switching optimal control problems (Xu & Antsaklis, 2003), such as the energy optimal problem when negative power is dissipated, where the running cost function has different expression when power is either positive or negative. This performance is reached by finding each sub-piece of the optimal trajectory analytically and then collected imposing boundary conditions (BCs). Lastly, experimental tests have been performed to evaluate the energy-saving capabilities of the proposed trajectories.

1.4. Paper organization

The remainder of this paper is organized as follows. The formulation of the problem is provided in Section 2. Section 3 presents algorithms for on-line computation of energy-optimal trajectories for the case in which negative power is regenerated, for both unconstrained and constrained cases. The solution of the more challenging problem with negative power dissipation is presented in Section 4. Numerical results in Section 5 demonstrate the benefits of the presented method. The experimental setup is presented in Section 6 while its identification is explained in Section 7. The experimental data are compared to the predicted ones in Section 8; conclusions are in Section 9.

2. Problem statement

2.1. Electro-mechanical model

Considering a DC motor (extension to permanent magnet synchronous motors is straightforward using the DC-equivalent model), its instantaneous power consumption can be computed as:

$$\mathcal{P} = v_a i_a \tag{1}$$

where v_a is the armature voltage drop and i_a is the armature current. Using the equivalent circuit model, the voltage drop is composed of two terms, one related to the copper losses and one to the back electromotive force:

$$v_a = R_a i_a + L_a \frac{\mathrm{d}i_a}{\mathrm{d}t} + k_v \dot{\vartheta} \tag{2}$$

where R_a and L_a are the resistance and inductance of the armature. k_v is the back electromotive force (EMF) constant and $\dot{\vartheta}$ is the motor angular velocity. The inductive term will be, however, neglected for the rest of this work, as it has been proved that it does not influence the energy consumption during the execution of rest-to-rest tasks (Richiedei & Trevisani, 2016), as is the case here.

The armature current and the torque τ delivered by the motor are related by the torque constant $i_a = \tau/k_t$. As known, numerically the torque constant is equal to the back EMF constant $k_t = k_v$. Considering a 1 DOF mechatronic system with linear dynamics, such as the ones shown in Fig. 1, the torque required by the motor is:

$$\tau = I\ddot{\vartheta} + F\dot{\vartheta} + C \tag{3}$$

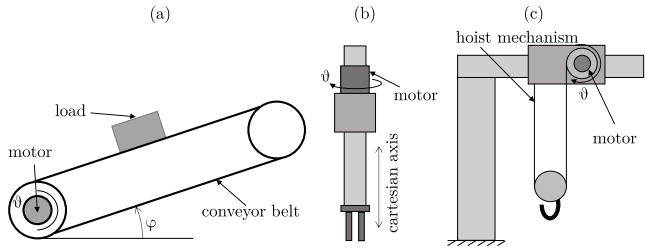

Fig. 1. Examples of mechatronic systems with linear dynamics: (a) belt-driven linear guide; (b) Cartesian robot; (c) hoist mechanism.

where I and F are the total inertia and the viscous friction coefficient of the system reduced to the motor axis, respectively. C is the constant torque required by the system to compensate the gravity and the Coulomb friction force, all reduced to the motor axis.

Substituting Eqs. (2) and (3) into Eq. (1) gives the following expression for the electric power absorbed by the motor, $\mathcal{P}$:

$$\mathcal{P} = R\ddot{\vartheta}^2 + Q\dot{\vartheta}^2 + \alpha\dot{\vartheta}\ddot{\vartheta} + \beta\dot{\vartheta} + \gamma\ddot{\vartheta} + \delta \tag{4}$$

where the coefficients are defined as follows:

$$\begin{aligned} R &= \frac{I^2\, R_a}{{k_t}^2}; \qquad Q = \left(F + \frac{F^2\, R_a}{{k_t}^2}\right) \\ \alpha &= \left(I + \frac{2\,F\,I\,R_a}{{k_t}^2}\right); \qquad \beta = \left(C + \frac{2\,C\,F\,R_a}{{k_t}^2}\right) \\ \gamma &= \frac{2\,C\,I\,R_a}{{k_t}^2}; \qquad \delta = \frac{C^2\, R_a}{{k_t}^2} \end{aligned} \tag{5}$$

2.2. Trajectory requirements

The focus of this work is on PTP motion, with rest-to-rest condition and with fixed motion time t_f. This means that the motion profile must satisfy the following BCs:

$$\begin{cases} \vartheta(0) = \vartheta_{\text{in}} \\ \vartheta(t_f) = \vartheta_{\text{fin}} \end{cases} \quad \begin{cases} \dot{\vartheta}(0) = 0 \\ \dot{\vartheta}(t_f) = 0 \end{cases} \quad \begin{cases} \ddot{\vartheta}(0) = 0 \\ \ddot{\vartheta}(t_f) = 0 \end{cases} \tag{6}$$

where ϑ_{in} and ϑ_{fin} are the initial and final values of the motor angular position, respectively. The conditions on the initial and final accelerations are introduced to avoid acceleration discontinuities at the beginning and at the end of the motion profile, as they would excite unwanted vibrations (Biagiotti & Melchiorri, 2008).

Further requirements are that the velocity, acceleration, and jerk must be bounded:

$$|\dot{\vartheta}(t)| \le v_{\text{lim}}; \quad |\ddot{\vartheta}(t)| \le a_{\text{lim}}; \quad |\dddot{\vartheta}(t)| \le j_{\text{lim}} \tag{7}$$

where j_{lim} is the maximum allowed jerk, v_{lim} and a_{lim} are the limits of velocity and acceleration. Those are typical requirements in industrial practice, as the enforcement of speed limits is needed to comply with the maximum speed ratings of actuators and of transmission devices. Acceleration limits actually allow to confine the maximum value of torque, given the direct proportionality between torque and acceleration in constant inertia systems. Finally, jerk limits, acceleration limits and acceleration continuity allow to confine the effects of motion-induced oscillations and mechanical stresses (Biagiotti & Melchiorri, 2008).

2.3. Problem formulation

The goal of the motion design procedure is the minimization of the energy consumption, which is defined as the time integral of the electric energy delivered to the motor. The dynamic model of the system under consideration must then be written as a first order dynamic systems, to comply with the intended use of a variational formulation. To do so, the problem is rewritten in state-space form. Let $[\vartheta,\ \dot{\vartheta}]^\top = [x_1,\ x_2]^\top = \mathbf{x}$ be the state vector and $\ddot{\vartheta} = u$ be the scalar control value. The dynamics of the system is:

$$\begin{cases} \dot{x}_1 = x_2 \\ \dot{x}_2 = u \end{cases} \tag{8}$$

by substituting the symbols of the state-space form, the power delivered to the motor can be rewritten as:

$$\mathcal{P} = Ru^2 + Qx_2^2 + \alpha x_2 u + \beta x_2 + \gamma u + \delta \tag{9}$$

hence, the optimal control problem at hand is:

$$\begin{aligned} \underset{u\in\mathcal{U}}{\text{minimize}} \quad & \mathcal{E} = \int_0^{t_f} \mathcal{P}(\mathbf{x}, u, t)\mathrm{d}t \\ \text{subject to:} \quad & \text{(6) and (7)} \\ & \dot{\mathbf{x}} = \mathbf{f}(\mathbf{x}, u, t) \end{aligned} \tag{10}$$

where $\mathcal{E}$ is the total electric energy expenditure, t_f is the prescribed final time and $\mathcal{U}$ is the space of the possible controls according to the constraints and BCs. Let t_{min} be the minimum time, according to the constraints, to perform the task. In this work, it is assumed that the assigned final time t_f is strictly greater than t_{min}. If $t_f < t_{\text{min}}$, there is clearly no solution. If $t_f = t_{\text{min}}$ the solution is coincident to the minimum time solution.

For a comprehensive explanation on how to calculate t_{min}, the reader might refer to Section 3.4.3 of the book (Biagiotti & Melchiorri, 2008).

It must be pointed out that the target of energy minimization is explicitly represented by setting the cost function as equal to the net energy consumption, as the minimization is of just the dissipated energy is, as mentioned in Section 1.2, not equivalent to a true energy cost minimization and is not compliant with the absence of a negative power regeneration device.

Given that several possibility can arise according to the choice of the motion execution times, several combinations of active constraints must be taken into consideration. As each additional constraint alters the shape of the optimal solution, all the possible cases are taken into consideration in the next section, and then the analysis is repeated for the case without regeneration.

3. Solution with negative power regeneration

This section consists of the following parts: in 3.1 the solution of the unconstrained problem is addressed; in 3.2 acceleration and jerk constraints are introduced; in 3.3 the velocity constraint is introduced. Note that a proof of the existence of the optimal solutions in these cases is provided in Wang et al. (2013).

3.1. Unconstrained solution

The problem stated in Eq. (10) can be solved using Pontryagin's maximum principle. The Hamiltonian of the system is:

$$\mathcal{H} = \mathcal{P} + \mathbf{p}^\top \mathbf{f} \tag{11}$$

where $\mathcal{P}$ is given by Eq. (4), $\mathbf{f}$ by Eq. (8), while $\mathbf{p} = [p_1,\ p_2]^\top$ is the vector of the co-states. The uniqueness of the solution of (10) is ensured by the convexity of the Hamiltonian w.r.t. the control. For simplicity, the unconstrained problem with only position and velocity BCs is examined at first. In fact, for a fixed final-time problem with n states, we must apply $2n$ BCs. The necessary conditions for strong extrema are provided by the Hamilton Canonical Equations:

$$\mathcal{H}_u = 0 \longrightarrow 2Ru + \alpha x_2 + \gamma + p_2 = 0 \tag{12}$$

$$\mathcal{H}_{x_1} = -\dot{p}_1 = 0 \longrightarrow p_1 = \text{const} \tag{13}$$

$$\mathcal{H}_{x_2} = -\dot{p}_2 = 2Qx_2 + \alpha u + \beta + p_1 \tag{14}$$

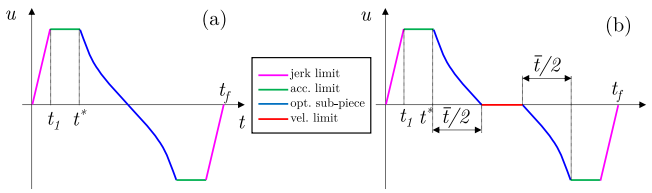

Fig. 2. Structure of the solution when negative power is regenerated: with active jerk and acceleration limits (a), with active jerk, acceleration and speed limits (b).

Eq. (12) can be the differentiated with respect to time, then $\dot{p}_2$ can be isolated and used into Eq. (14), leading to:

$$2Qx_2 + \cancel{\alpha u} + \beta + p_1 = 2R\dot{u} + \cancel{\alpha \dot{x}_2} \tag{15}$$

where the cancellation is made upon the observation that $\dot{x}_2 = u$ from Eq. (8). By observing that $\dot{u} = \ddot{x}_2$ and that p_1 and β are constants, Eq. (15) leads to the following second order differential equation:

$$\ddot{x}_2 - \frac{Q}{R}x_2 = \frac{p_1 + \beta}{2R} \tag{16}$$

A solution to Eq. (16) can be obtained as the sum of the solution of the associated homogeneous equation $x_{2,h}$ and of the particular solution $x_{2,p}$. Defining $\lambda^2 = Q/R$, such solution is:

$$x_2 = x_{2,h} + x_{2,p} = Ae^{\lambda t} + Be^{-\lambda t} - \frac{p_1 + \beta}{2Q} \tag{17}$$

that, integrated with respect to time, gives x_1:

$$x_1 = \frac{A}{\lambda}e^{\lambda t} - \frac{B}{\lambda}e^{-\lambda t} - \frac{p_1 + \beta}{2Q}t + c \tag{18}$$

where c is a constant of integration. In addition, the expression of the optimal control is:

$$u = A\lambda e^{\lambda t} - B\lambda e^{-\lambda t} \tag{19}$$

Now, by using the BCs for the state vector $\mathbf{x}$ as they are reported in Eq. (6):

$$\begin{aligned}
&x_1(0) = \vartheta_i \rightarrow \frac{A}{\lambda} - \frac{B}{\lambda} + c = \vartheta_i \\
&x_1(t_f) = \vartheta_f \rightarrow \frac{A}{\lambda}e^{\lambda t_f} - \frac{B}{\lambda}e^{-\lambda t_f} - \frac{p_1 + \beta}{2Q}t_f + c = \vartheta_f \\
&x_2(0) = 0 \rightarrow A + B - \frac{p_1 + \beta}{2Q} = 0 \\
&x_2(t_f) = 0 \rightarrow Ae^{\lambda t_f} + Be^{-\lambda t_f} - \frac{p_1 + \beta}{2Q} = 0
\end{aligned} \tag{20}$$

the above equations can be condensed as the following linear system:

$$\begin{bmatrix} \frac{1}{\lambda} & -\frac{1}{\lambda} & 0 & 1 \\ \frac{1}{\lambda}e^{\lambda t_f} & -\frac{1}{\lambda}e^{-\lambda t_f} & -\frac{t_f}{2Q} & 1 \\ 1 & 1 & -\frac{1}{2Q} & 0 \\ e^{\lambda t_f} & e^{-\lambda t_f} & -\frac{1}{2Q} & 0 \end{bmatrix} \begin{bmatrix} A \\ B \\ p_1 \\ c \end{bmatrix} = \begin{bmatrix} \vartheta_{\text{in}} \\ \vartheta_{\text{fin}} + \frac{\beta}{2Q}t_f \\ \frac{\beta}{2Q} \\ \frac{\beta}{2Q} \end{bmatrix} \tag{21}$$

Once A, B, p_1 and c are obtained, the trajectory is completely determined. This solution is the one to be used for the simple case in which none of the velocity, acceleration and jerk constraints are active, i.e. for 'large' values of t_f. This solution will also be used as the basis for the development of the analytical solutions to be used for the various scenarios cited above.

3.2. Finite jerk/acceleration limit solution

Infinite values of jerk should be avoided to reduce the frequency content of the trajectory (Biagiotti & Melchiorri, 2008). To do so, acceleration should be continuous for the whole trajectory, and null at initial an final times as well. Any violation to these condition introduce a jerk impulse. The design of the motion profile will therefore enforce these conditions as well.

The necessary conditions for optimal trajectory with control constraints can be formulated in different ways. For instance, the work Bryson and Ho (2018) suggests to embed the constraints in the Hamiltonian by augmenting it, but this kind of method exposes some unnecessary challenges to the formulation and to the solution of the problem, which are avoided by the method proposed here.

As shown in Wang et al. (2013, 2014), the solution with acceleration limits exhibits a three-phase structure: an acceleration-constrained first piece, an unconstrained central part, and an acceleration-constrained final piece. In this work, instead of solving the augmented Hamiltonian, the BCs for each individual section of the trajectory are exploited to evaluate the duration of each phase of the trajectory. Those conditions are sufficient to ensure optimality since no other law with the prescribed structure satisfies the requirements for optimality.

Let us consider Fig. 2a, which shows the structure of the optimal control for only jerk and acceleration active constraints, and let t^* be the duration of the first segment. This piece is made up of a finite jerk arc of equation $u = j_{\text{lim}}t$; if this piece lasts longer than $t_1 = a_{\text{lim}}/j_{\text{lim}}$ then the control assumes a constant value of $u = a_{\text{lim}}$. Since the control solution is anti-symmetric with respect to half-time, the first and last pieces have equal lengths. The central piece is the optimal law that minimizes the energy expenditure using the BCs given by the first and last constrained pieces. It is sufficient to update the BCs in Eq. (6) and substituting t_f with $t_f - 2t^*$ in Eq. (21). The linear system to be solved is:

$$\begin{bmatrix} \lambda & -\lambda & 0 \\ 1 & 1 & -\frac{1}{2Q} \\ e^{\lambda t_f^*} & e^{-\lambda t_f^*} & -\frac{1}{2Q} \end{bmatrix} \begin{bmatrix} A \\ B \\ p_1 \end{bmatrix} = \begin{bmatrix} \min\left[a_{\text{lim}}, j_{\text{lim}}\, t^*\right] \\ \frac{\beta}{2Q} + \dot{\vartheta}^* \\ \frac{\beta}{2Q} + \dot{\vartheta}^* \end{bmatrix} \tag{22}$$

where $\dot{\vartheta}^*$ is the velocity at the end of the constrained phase and $t_f^* = t_f - 2t^*$. The constant c can be easily obtained by imposing the position BCs at the beginning. t^*, which appears in (22), is not known *a priori*: to find it, it is sufficient to solve a root-finding problem. If ϑ^* is the distance covered during each constrained part of the motion — i.e. between $t = 0$ and t^*, and between $t_f - t^*$ and t_f, the remaining distance to be traveled during the non-constrained part can be referred to a $\Delta\vartheta_{\text{opt}}$. Since these three pieces, as already discussed, compose the whole trajectory, the following can be stated:

$$\Delta\vartheta = \vartheta_{\text{fin}} - \vartheta_{\text{in}} = 2\Delta\vartheta^* + \Delta\vartheta_{\text{opt}} \tag{23}$$

the analytic formulation of the distance $\Delta\vartheta_{\text{opt}}$ can be found by double integration over time of the control for the central section of the motion profile as:

$$\Delta\vartheta_{\text{opt}} = \frac{A}{\lambda}e^{\lambda t_f^*} - \frac{B}{\lambda}e^{-\lambda t_f^*} - \frac{p_1 + \beta}{2Q}t_f^* - \frac{A}{\lambda} + \frac{B}{\lambda} \tag{24}$$

where $t_f^* = t_f - 2t^*$. The angle spanned during the initial and final constrained phase $\Delta\vartheta^*$ is the same for symmetry. The expression for $\Delta\vartheta^*$ can take two different values, one for $t^* < t_1$ and the other for $t^* > t_1$. The formulas to be used are:

$$\Delta\vartheta^* = \frac{1}{2}j_{lim}t_1\left(t^{*2} - t_1t^* + \frac{1}{3}t_1^2\right); \quad \text{for } t^* < t_1 \tag{25}$$

and

$$\Delta\vartheta^* = \frac{1}{6}j_{lim}t^{*3}; \quad \text{for } t^* > t_1. \tag{26}$$

Finally, t^* can be found numerically, i.e. using Newton's method, by solving Eq. (23), in which Eq. (24) is used together with either Eq. (25) or Eq. (26), as in:

$$\Delta\vartheta - 2\Delta\vartheta^* - \Delta\vartheta_{\text{opt}} = f(t^*) = 0 \tag{27}$$

3.3. Velocity limit

The activation of the speed limit in addition to the jerk and acceleration limit imposes a further constraints which alters the general structure of the control action, which is shown in Fig. 2(b). The comparison with the left part of the same figure highlights the additional of a further segment, shown in red, during which the speed is constant and equal to v_{lim} and the control action — i.e the acceleration, as well as the jerk, are null.

Always referring to Fig. 2(b), t^* is the time at which the unconstrained part of the optimal control starts (i.e. the start of the first blue part): this section is however interrupted by the velocity limit section, and the total duration of the two blue parts, is now measured as $\bar{t}$. The two values t^* and $\bar{t}$ define uniquely the optimal motion profile.

Two conditions can be enforced to find their values: (i) the overall displacement must be equal to the desired one, as imposed in Section 3.2; (ii) the maximum velocity of the optimal sub-piece must be equal to the limit velocity v_{lim}.

Given that optimality must be obtained along the whole motion, it can be recognized that the analytic expression for the motion in each section in which no constraint is active (i.e. during each of the two 'blue' sections) must be equal to the same one to be used without the active velocity limits (i.e. when there is only one 'blue' section), with the only difference being the BCs for each unconstrained part. Fig. 2(b) highlights that the control action for the first unconstrained part is subject to two BCs, the first one being the position, speed and acceleration continuity at t^*, and the other one is that, at $t^* + \bar{t}/2$ speed must be equal to v_{lim}, and acceleration must be zero. The second unconstrained part is then symmetrical, with the obvious considerations to such BCs.

Recalling some useful formulas, the acceleration at t^* must be equal to:

$$\lambda A - \lambda B = a_{\text{lim}} \tag{28}$$

Another condition is that the initial and final velocities must to be equal to the final and initial velocity of the first and last constrained piece. Since those velocities are equal from symmetry considerations, it is sufficient to impose that the initial and the final velocities of the optimal piece must be the same. By using the temporal variable $\bar{t}$ that is zero at the beginning of the optimal sub-piece and considering the first and the second sub-piece together, this condition can be written as:

$$A + B - \cancel{\frac{p_1 + \beta}{2Q}} = Ae^{\lambda\bar{t}} + Be^{-\lambda\bar{t}} - \cancel{\frac{p_1 + \beta}{2Q}} \tag{29}$$

Eqs. (28) and (29) form a linear system in the unknowns A and B. To define the velocity law, the co-state p_1 can be found by imposing the continuity of velocity at the beginning of the optimal sub-piece:

$$A + B - \frac{p_1 + \beta}{2Q} = a_{\text{lim}} t^* - \frac{1}{2} j_{\text{lim}} t_1^2 \tag{30}$$

The condition on the maximum velocity of the optimal sub-piece can be stated as follows:

$$Ae^{\lambda\bar{t}/2} + Be^{-\lambda\bar{t}/2} - \frac{p_1 + \beta}{2Q} - v_{\text{lim}} = f(t^*, \bar{t}) = 0 \tag{31}$$

The second condition is that the trajectory must provide the requested overall displacement $\Delta\vartheta$, which can be formalized in accordance to the procedure already used in Eq. (23), as:

$$2\Delta\vartheta^* + \Delta\vartheta_{\text{opt}} + \Delta\vartheta_{\dot{\vartheta}=v_{\text{lim}}} - \Delta\vartheta = g(t^*, \bar{t}) = 0 \tag{32}$$

in which $\Delta\vartheta^*$ is the displacement associated with the first and last part – i.e. when jerk and acceleration limits are active – which can be evaluated as:

$$\Delta\vartheta^* = \frac{1}{2} j_{\text{lim}} t_1 \left(t^{*2} - t_1 t^* + \frac{1}{3} t_1^2 \right) \tag{33}$$

Then $\Delta\vartheta_{\text{opt}}$ can be evaluated as:

$$\Delta\vartheta_{\text{opt}} = \frac{A}{\lambda} e^{\lambda\bar{t}} - \frac{B}{\lambda} e^{-\lambda\bar{t}} - \frac{p_1 + \beta}{2Q}\bar{t} - \frac{A}{\lambda} + \frac{B}{\lambda} \tag{34}$$

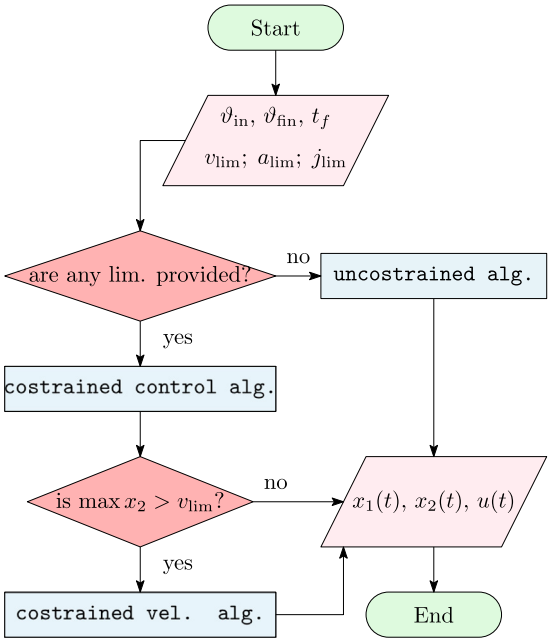

Fig. 3. Explanation of the negative power regeneration algorithm.

During the constant velocity phase (i.e. the 'red' part), the displacement is defined as:

$$\Delta\vartheta_{\dot{\vartheta}=v_{\text{lim}}} = v_{\text{lim}}(t_f - 2t^* - \bar{t}) \tag{35}$$

Finally, t^* and $\bar{t}$ are found by numerically solving the nonlinear system of Eqs. (31) and (32), again using e.g. the generalized Newton's method or any other suitable method. This formulas complete all the possible cases when energy regeneration is assumed. A complete picture of the algorithm, considering all the situations presented in this section, is depicted in Fig. 3.

4. Solution with negative power dissipation

Now the case of negative power dissipation is analyzed: this refers to the case in which no practical means are available to store or to deliver to another device the regenerated power, which therefore must be dissipated by a braking resistor. Given the definition of the electric power of Eq. (1), electric power is positive when absorbed, and negative when generated by the motor itself, which acts as a regenerative brake. Regenerated energy is in this case dissipated, and therefore negative values of $\mathcal{P}$ must be neglected when computing the energy cost according to Eq. (10). As a consequence, the *running cost* must be defined as a switching function, as follows:

$$\mathcal{P}(\mathbf{x}, u, t) = \begin{cases} \mathcal{P}(\mathbf{x}, u, t); & \text{if} \quad \mathcal{P}(\mathbf{x}, u, t) > 0 \\ 0; & \text{otherwise} \end{cases} \tag{36}$$

since the negative values of the electric part must be discarded when computing the energy cost according to Eq. (10). The switch in the function $\mathcal{P}$ extends to the cost function $\mathcal{E}$, and as a consequence, to the Hamiltonian as well.

Two particular cases are studied in Sections 4.1 and 4.2, one in which the finite jerk and acceleration limit constraints are active and the other in which the velocity limit constraint is active as well. The two particular cases are studied because the structure of the solution is different to the one analyzed so far, because of the switches of the Hamiltonian that happen whenever the absorbed electric power changes sign, as a consequence of the change in the cost function, according to Eq. (11).

4.1. Finite jerk/acceleration limit solution

Let us consider the situation in which the total execution time t_f is small enough to ensure that jerk and acceleration constraints are active, maximum speed is not reached, and negative power is being dissipated rather then being regenerated. As shown in Fig. 4a, the solution is composed by four main pieces. The first part is the constrained jerk and acceleration section that is fully defined by knowing t^*, which has been discussed in detail in the previous section. After that, there is an optimal sub-piece with the same structure of Eq. (17), which however ends when the absorbed electric power gets null: this event triggers the Hamiltonian switch and the power is equal to zero. Another Hamiltonian switch is found when the electric power gets positive again, which ends the 'null power' section, which is depicted in brown color in Fig. 4a. The last section consists of a jerk-acceleration-jerk constrained part.

The solution can be parameterized by t^*, t_o^* and t_{so}, as reported in Fig. 4a. The procedure used to find them employs the enforcement two continuity conditions and the solution to a minimization problem in one variable.

Before imposing the conditions, the time t_m at which the switch of the Hamiltonian occurs should be evaluated. It is sufficient to impose that the power equals zero by using the equation of acceleration and velocity given by (17) and solving it for the time. The resulting equation will be of the algebraic type and its solution is not trivial. However, since power is the product of the armature current and the armature voltage, zero power means either zero current or zero voltage. If the current is zero then the voltage cannot be zero and vice-versa, since $v_a = R_a i_a + k_v \dot{\vartheta}$, unless current is negative, but actually before reaching a negative value, it reaches, as obvious, a null value. Initially, both velocity and torque (hence current) are positive. To have zero voltage, either current or velocity has to be negative. Since velocity is never negative, current has to be negative. But if torque is initially positive and is continuous (because derived by composition of continuous functions), by Bolzano's theorem it will be zero before being negative. Hence, the condition is that $\tau = I\ddot{\vartheta} + F\dot{\vartheta} + C = 0$. By substituting the expressions for velocity and acceleration:

$$I\left(\lambda A e^{\lambda t} - \lambda B e^{-\lambda t}\right) + F\left(A e^{\lambda t} + B e^{-\lambda t} - \frac{p_1+\beta}{2Q}\right) + C = 0 \tag{37}$$

The equation above is algebraic, but substituting $z = e^{\lambda t}$ leads to :

$$\frac{\alpha_1 z^2 + \alpha_2 z + \alpha_3}{z} = 0 \tag{38}$$

where:

$$\alpha_1 = 2AQ(F + I\lambda); \quad \alpha_2 = 2CQ - F(p_1+\beta); \quad \alpha_3 = 2BQ(F - I\lambda); \tag{39}$$

By solving the second-order equation, one can find:

$$t_m = \log(z)/\lambda \tag{40}$$

If $t_m > t_{so}$ the solution does not exhibit the switch and therefore the method developed for the regenerative case should be used. As already discussed, the null power condition is equivalent to the following:

$$\tau = I\ddot{\vartheta}(t) + F\dot{\vartheta}(t) + C = 0 \tag{41}$$

which, in terms of state space variables, is:

$$x_2 = \dot{\vartheta} = c_1 e^{-F/I t} - \frac{C}{F} \tag{42}$$

The integration constant c_1 can be found by imposing the continuity of velocity. The continuity of acceleration is ensured by the fact that the point at which the switch occurs satisfies Eq. (37), which is a punctual case of Eq. (41). Since the analytic expression for all the trajectory segments are found, it is now sufficient to find the time durations of each of them to define the whole solution. As done before, the time durations are found by enforcing some conditions on the displacements which happen during the several phases of the motion.

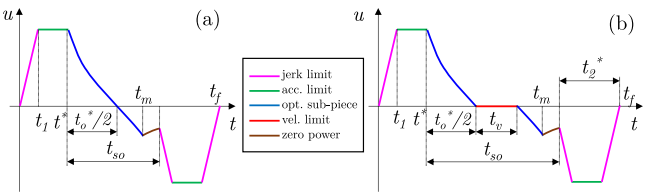

Fig. 4. Structure of the solution when negative power is dissipated. Left side (a) refers to the case in which jerk and acceleration constraints are active while right side (b) to when the velocity constraint is active as well.

The first condition is that the total displacement has to be equal to the prescribed one, as done in Section 3.2 using Eq. (27). The displacement of the first piece, i.e. the constrained piece from 0 to t^*, is the same of $\Delta\vartheta^*$ in Eq. (27). The second displacement $\Delta\vartheta_{\text{opt},1}$ is the first optimal piece. It can be found by integrating the velocity x_2 from 0 to t_m:

$$\begin{aligned}\Delta\vartheta_{\text{opt},1} &= \int_0^{t_m}\left(A e^{\lambda t} + B e^{-\lambda t} - \frac{p_1+\beta}{2Q}\right)\mathrm{d}t = \\ &= \frac{A}{\lambda}e^{\lambda t_m} - \frac{B}{\lambda}e^{-\lambda t_m} - \frac{p_1+\beta}{2Q}t_m - \frac{A}{\lambda} + \frac{B}{\lambda}\end{aligned} \tag{43}$$

the third displacement $\Delta\vartheta_{\text{opt},2}$ is given by the optimal solution after the Hamiltonian switch. To find it, it is sufficient to integrate Eq. (41) from t_m to the end of the optimal sub-piece, t_{so}:

$$\begin{aligned}\Delta\vartheta_{\text{opt},2} &= \int_{t_m}^{t_{so}}\left(c_1 e^{-\frac{F}{I}t} - \frac{C}{F}\right)\mathrm{d}t = \\ &= -\frac{c_1}{F/I}e^{-\frac{F}{I}t_{so}} + \frac{c_1}{F/I}e^{-\frac{F}{I}t_m} - \frac{C}{F}(t_{so} - t_m)\end{aligned} \tag{44}$$

the last piece $\Delta\vartheta_2^*$ refers to the constrained part:

$$\Delta\vartheta_2^* = \frac{1}{2}j_{\lim}t_1^2 + a_{\lim}(t^* - t_1) + \frac{1}{2}(t_2^* - t^*)(a_{\lim} - u(t_{so})) \tag{45}$$

and, finally:

$$(\vartheta_{\text{fin}} - \vartheta_{\text{in}}) - \Delta\vartheta^* - \Delta\vartheta_{\text{opt},1} - \Delta\vartheta_{\text{opt},2} - \Delta\vartheta_2^* = f(t^*, t_o^*, t_{so}) = 0 \tag{46}$$

another condition is the need to ensure zero velocity at end of the trajectory. To do this, considering that initial speed is always zero, the time integral of the acceleration profile must be zero as well. Since the velocity of the optimal piece is continuous and determined imposing BCs in $t = t^*$, the condition has to focus only on the velocities in $t = t^* + t_{so}$, as follows:

$$x_{2,o}(t_{so} + t^*) - x_{2,f}(t_{so} + t^*) = g(t^*, t_o^*, t_{so}) = 0 \tag{47}$$

where $x_{2,o}(t_{so} + t^*)$ is the velocity at the end of the optimal arc and $x_{2,f}(t_{so} + t^*)$ is the velocity at the beginning of the last constrained arc. When the conditions given by Eqs. (46) and (47) are imposed, the resulting trajectory satisfies all the desired constraints and conditions.

As discussed so far, two conditions are imposed, but three parameters are instead needed to completely define the trajectory. To find the last parameter, an optimization problem in one variable can be solved:

$$\underset{t_{so}}{\text{minimize}} \quad \mathcal{E} = \int_0^{t_f}\mathcal{P}(\mathbf{x}, u, t)\mathrm{d}t \tag{48}$$

subject to (46) and (47)

this problem is solved using the `fminbnd` Matlab's function, exploiting the t_{so} has to be in the $(0,\ t_f)$ range. The solution of Eq. (48) completes the solution of the optimal control problem, hence the design of the optimal motion profile in the absence of electric energy regeneration.

4.2. Velocity limit

If the results of Section 4.1 does violate the velocity limit, the structure of the solution changes according to Fig. 4b, which requires

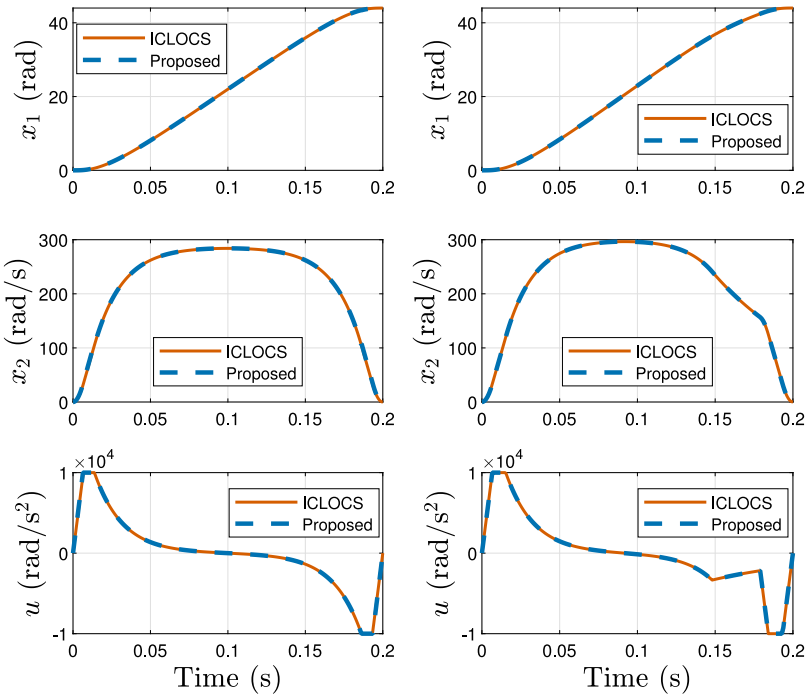

Fig. 5. Solutions when only jerk and acceleration constraints are active: (left) negative power regeneration case; (right) negative power dissipation case.

Table 1
System and motor data.

Parameter	Unit	Value
I	kg m^2	$7.2 \cdot 10^{-5}$
F	Nms/rad	$1 \cdot 10^{-3}$
C	Nm	0.0
R_a	Ω	5.0
k_t	Nm/A	0.27

Table 2
Comparison of computational times: mean values μ and standard variation σ. Note that the quantity for ICLOCS2 are expressed in seconds while milliseconds are used for the proposed method.

reg	$v_{\lim}$	ICLOCS2		Proposed method	
		μ_I (s)	σ_I (s)	μ_P (ms)	σ_P (ms)
✓	✗	224.6	118.0	1.73	0.05
✓	✓	1786.6	1018.7	5.87	0.05
✗	✗	34.2	14.2	23.3	3.9
✗	✓	30.8	10.0	47.3	5.9

the additional parameter t_v, i.e. the time length during which the velocity constraint is active. Since it is not known *a priori* whenever the velocity limit is hit or not, the algorithm explained in this section is intended to be performed after the one explained in Section 4.1 in the case in which $\max_t(x_2) > v_{\lim}$. The condition on the overall displacement given by Eq. (46) changes to:

$$(\vartheta_{\text{fin}} - \vartheta_{\text{in}}) - \Delta\vartheta^* - \Delta\vartheta_{\text{opt},1} - \Delta\vartheta_{\text{opt},2} - \Delta\vartheta_2^* - \Delta\vartheta_v = f(t^*, t_{\text{o}}^*, t_{\text{so}}, t_v) = 0 \tag{49}$$

where $\Delta\vartheta_v = v_{\lim} t_v$. In contrast, the condition on velocities is the same as in Eq. (47). The additional equation is given by Eq. (31), where $\bar{t}$ should be replaced by t_{o}^*.

5. Numerical results

This section presents some numerical examples, obtained using MATLAB, running on a Windows PC equipped with an AMD Ryzen 4500U processor and 8 GB of RAM. The motor and system parameters used are listed in Table 1. The total displacement in all cases is $\Delta\vartheta = 44$ rad. The trajectory limits are set to $v_{\lim} = 100\pi$ rad/s, $a_{\lim} = 10^4$ rad/s^2 and $j_{\lim} = 1.5 \cdot 10^6$ rad/s^3.

Fig. 5 shows the solutions for $t_f = 0.20$ s, with active jerk and acceleration constraints, for both the regenerative braking case and the negative power dissipation case. In Fig. 6 the task time is then reduced to $t_f = 0.185$ s to trigger the velocity limit too. Both the cases with and without power regeneration are taken into consideration. The results are compared with the solution provided by an open source optimal control toolbox, ICLOCS2 (Nie, Faqir, & Kerrigan, 2018), whose capabilities were tested in various domains. As depicted in Figs. 5 and 6, there is a clear overlap between the proposed solutions and the ones obtained by solving the same optimization problems using ICLOCS2, which supports the correctness of the proposed solution.

The proposed method's main advantage over using ICLOCS2 is highlighted in Table 2, which lists the computational times required for planning optimal motion profiles. Six trials were conducted for each method, totaling $6 \times (4 + 4) = 24 + 24$ trials.

Table 2 displays mean values and standard deviations. ICLOCS2 demands an higher significant computational effort with times ranging from approximately 30 seconds to 30 minutes. In contrast, the proposed method achieves a dramatic speedup, with computational times averaging 1.73 ms in the best case and 47.3 ms in the worst case.

In all cases the solution times are sensibly smaller than the actual motion execution time, which supports the definition of the proposed method as Real-Time capable. It is indeed possible to plan each motion just before its execution without affecting the overall time needed by the sequential planning and execution phases.

6. Experimental setup

The effectiveness of the proposed trajectories are validated through several experimental tests. The mechatronic system is composed by a Escap 35NT2R82-426SP Brushed DC Motor that run a shaft and a PLA 3D printed flywheel. A picture of the physical system is reported in Fig. 7 The system is controlled by a Teensy 4.1 microcontroller and

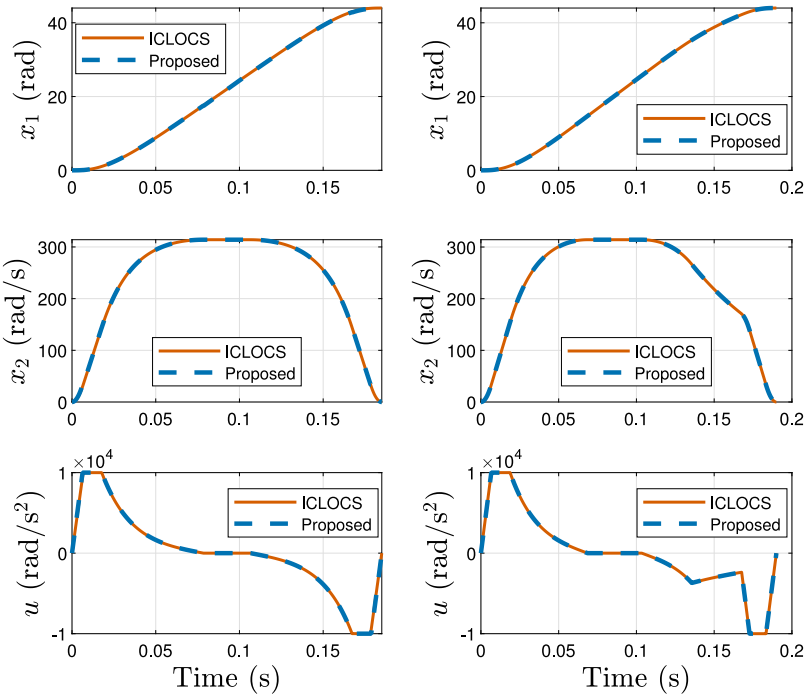

Fig. 6. Solutions for the velocity constrained cases: (left) regenerative braking case; (right) negative power dissipation case.

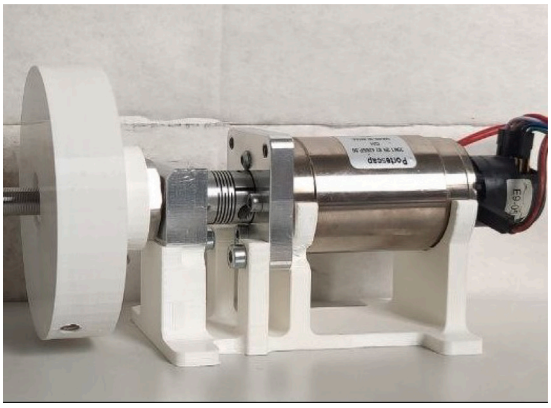

Fig. 7. Experimental setup, composed by a shaft and a flywheel actuated by an Escap 35NT2R82-426SP brushed DC Motor.

a AMC 25A8 DC motor driver. The driver is used in voltage mode and the operating frequency of the microcontroller is set to 1 kHz. The current and the voltage fed to the motor are measured with the National Instruments module NI cRIO-9215, with sampling frequency set to 10 kHz. The control scheme consists of a PID feedback controller augmented with a feed-forward controller, as shown in Fig. 8.

7. Identification procedure

A system identification procedure has been performed to obtain accurate values for the physical parameters of the electro-mechanical system. First the electrical data are identified collecting triplets of armature current i_a, armature voltage v_a and motor velocity $\dot{\vartheta}$. Using Eq. (2) without considering the inductive term, it is possible to write all the sampled triplets in matrix form, as follows:

$$\begin{bmatrix} \vdots \\ v_a(t_i) \\ \vdots \end{bmatrix} = \begin{bmatrix} \vdots & \vdots \\ i_a(t_i) & \dot{\vartheta}(t_i) \\ \vdots & \vdots \end{bmatrix} \begin{bmatrix} R_a \\ k_t \end{bmatrix} \tag{50}$$

which can be condensed as is:

$$\boldsymbol{v}_a = \boldsymbol{\Phi}_{\mathrm{e}} \boldsymbol{\pi}_e \tag{51}$$

where $\mathbf{v}_a$ is the vector collecting all the sampled voltages, $\boldsymbol{\Phi}_{\mathrm{e}}$ is the regressor matrix, whose column are the sampled currents and velocities and $\boldsymbol{\pi}_{\mathrm{e}} = [R_a, k_t]^\top$ collects the parameters to be estimated. The latter can be estimated as:

$$\boldsymbol{\pi}_{\mathrm{e}} = \boldsymbol{\Phi}_{\mathrm{e}}^{\dagger} \mathbf{v}_a \tag{52}$$

where with the † symbol represents the Moore–Penrose pseudoinverse. With the same method is possible to identify the inertia I, the viscous friction F and the constant friction torque C as well, recalling that:

$$\tau = I\ddot{\vartheta} + F\dot{\vartheta} + C \tag{53}$$

which, in turn, is condensed as:

$$\boldsymbol{\tau} = \boldsymbol{\Phi}_{\mathrm{m}} \boldsymbol{\pi}_{\mathrm{m}} \tag{54}$$

where $\boldsymbol{\tau}$ is the vector collecting the torques, $\boldsymbol{\Phi}_{\mathrm{m}} = [\ddot{\boldsymbol{\vartheta}}\ \dot{\boldsymbol{\vartheta}}\ \mathbf{1}]$ is the regressor matrix for the mechanical parameter and $\boldsymbol{\pi}_{\mathrm{m}} = [I, F, C]^\top$ is the vector of parameters to be estimated, using the expression:

$$\boldsymbol{\pi}_{\mathrm{m}} = \boldsymbol{\Phi}_{\mathrm{m}}^{\dagger} \boldsymbol{\tau} \tag{55}$$

with the estimated parameter is possible to generate the optimal trajectories and to improve the feed-forward action of the control.

8. Experimental results

The experimental parameters estimated using the methodology explained in Section 7 are listed in Table 3.

Five different trajectories were tested of which four were generated with the proposed method and the last is a standard symmetrical trapezoidal velocity law with acceleration ratio $\tau_a = 0.2$,[1] which is the ratio between the acceleration time and the total time t_f. The final time t_f is fixed for all the tests and is set to 2.3 s. Each type of

[1] It is a typical choice in the default settings of commercial servo systems.

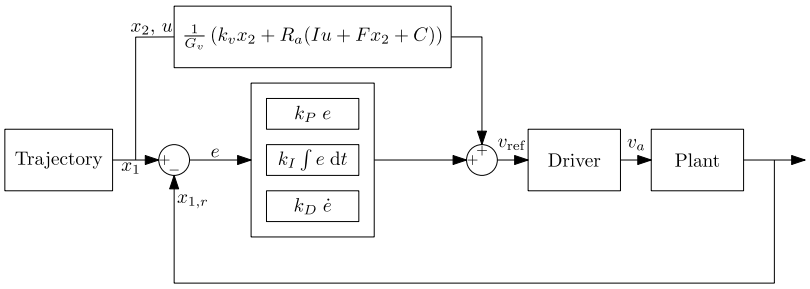

Fig. 8. Control scheme. G_v is the driver gain, $x_{1,r}$ is the measured position.

Table 3
Estimated parameter of the experimental setup.

Parameter	Unit	Value
I	kg m^2	$2.08 \cdot 10^{-6}$
F	Nms/rad	$3.37 \cdot 10^{-7}$
C	Nm	$7.03 \cdot 10^{-5}$
R_a	Ω	53.9
k_t	Nm/A	$5.18 \cdot 10^{-4}$

Table 4
Summary of the experimental trajectories tested. With `optreg`, `optdis` and `trap` the optimal case with regeneration, dissipation and the trapezoidal law are intended. The error is calculated for both the cases ($\text{err}_{\mathcal{E}}$ and $\text{err}_{\hat{\mathcal{E}}}$) with respect to the theoretical expected value. σ and $\hat{\sigma}$ are the standard deviation for the energy, with and without regeneration, respectively.

Test #	1	2	3	4	5
Type	`optreg`	`optreg`	`optdis`	`optdis`	`trap`
t_f (s)	2.3	2.3	2.3	2.3	2.3
j_{lim}	✓	✓	✓	✓	–
a_{lim}	✓	✓	✓	✓	–
v_{lim}	✓	✗	✓	✗	–
$\mathcal{E}$ (mJ)	29.03	29.49	30.02	29.65	34.18
σ (mJ)	0.10	0.08	0.19	0.17	0.11
$\hat{\mathcal{E}}$ (mJ)	38.52	38.62	34.58	34.68	46.93
$\hat{\sigma}$ (mJ)	0.10	0.08	0.19	0.19	0.11
$\text{err}_{\mathcal{E}}$ (%)	1.2	2.6	0.8	0.5	2.1
$\text{err}_{\hat{\mathcal{E}}}$ (%)	1.8	2.6	3.2	2.5	2.1

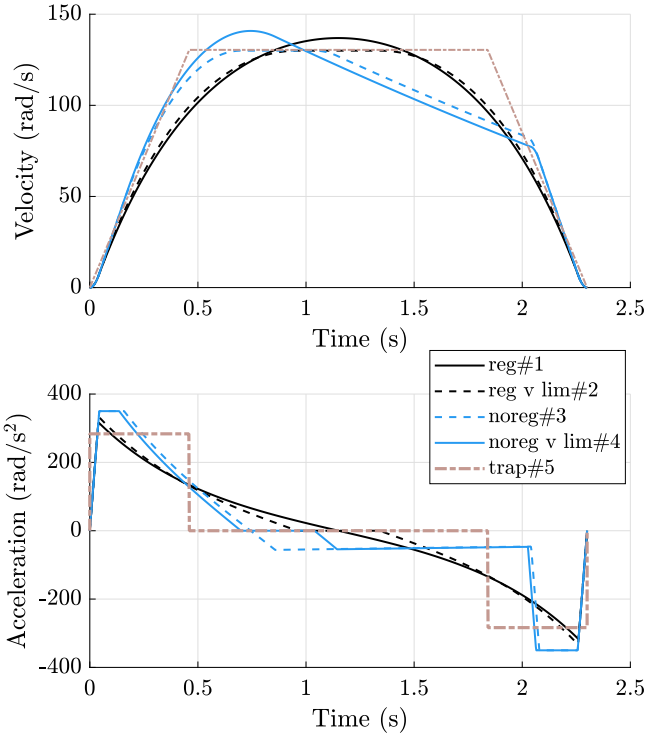

Fig. 9. Trajectories tested.

solution (the negative power (a) regeneration and (b) dissipation case) has been performed with and without the velocity limit. A summary of the tested trajectories is reported in Fig. 9 while the experimental results are summarized in Table 4.

Each test has been performed 100 times, and the results were averaged over time in order to reduce the effects of measurement noise. The trajectory limits are reported below:

$$v_{\text{lim}} = 130\,\text{rad/s};\ a_{\text{lim}} = 350\,\text{rad/s}^2;\ j_{\text{lim}} = 8000\,\text{rad/s}^3; \tag{56}$$

$\mathcal{E}$ is the measured energy expenditure assuming regeneration, while $\hat{\mathcal{E}}$ is the one evaluated assuming that no regeneration is available, i.e. neglecting the negative power values when evaluating the time integral that defines the energy absorption.

The effectiveness of the control scheme is corroborated by the fact that the mean position error that is equal to $7 \cdot 10^{-3}$ rad, a value which is comparable to the encoder resolution. $\text{err}_{\mathcal{E}}$ measures the difference between the theoretical and the experimentally measured energy consumption assuming regeneration, while $\text{err}_{\hat{\mathcal{E}}}$ is the same but with the assumption of no regeneration. Such errors are rather small in magnitude, being the worst estimation affected by just 3.2% error, which is reputed to be more than adequate considering also the simplicity of the setup. The slightly lesser accuracy found for the non regenerative case is mainly due to the non trivial detection of the negative power conditions due to the noise that affect the electric measurements. The energy efficiency improvement shown by comparison to the benchmark trapezoidal speed profile is also relevant, as reported in Table 4: with regeneration the energy cost improvement is at least equal to 12.17%, without regeneration the same figure increases to at least 17.71%. This results supports the effectiveness and the importance of the proposed investigation. The effectiveness in achieving a consistent energy improvement is also supported by the very limited standard deviations measured over 100 trials, as the standard deviations on the energy cost is, in all cases, below 0.2 mJ. The experimental results in terms of motion profiles and measured electrical quantities are reported in Figs. 10–14: the five figures show all the four optimized cases, plus the case concerning the non optimized trapezoidal motion profile.

9. Conclusions

In this work a method to design energy-efficient motion profiles for the rest-to-rest motion of servo-actuated systems with 1 DOF is proposed. The method can handle both systems with and without regenerative braking capability, and can take into account bounds on speed, acceleration and jerk.

The solution is developed separately for both the cases in which negative electric power is either regenerated or dissipated, given that its analytic form is different due to the switching nature of the cost

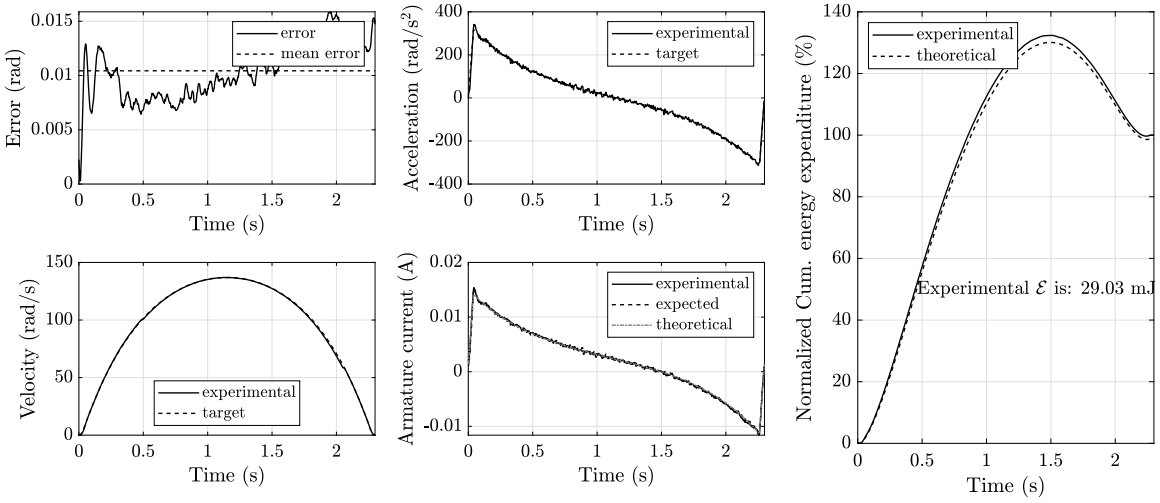

Fig. 10. Test # 1: regeneration without velocity limit.

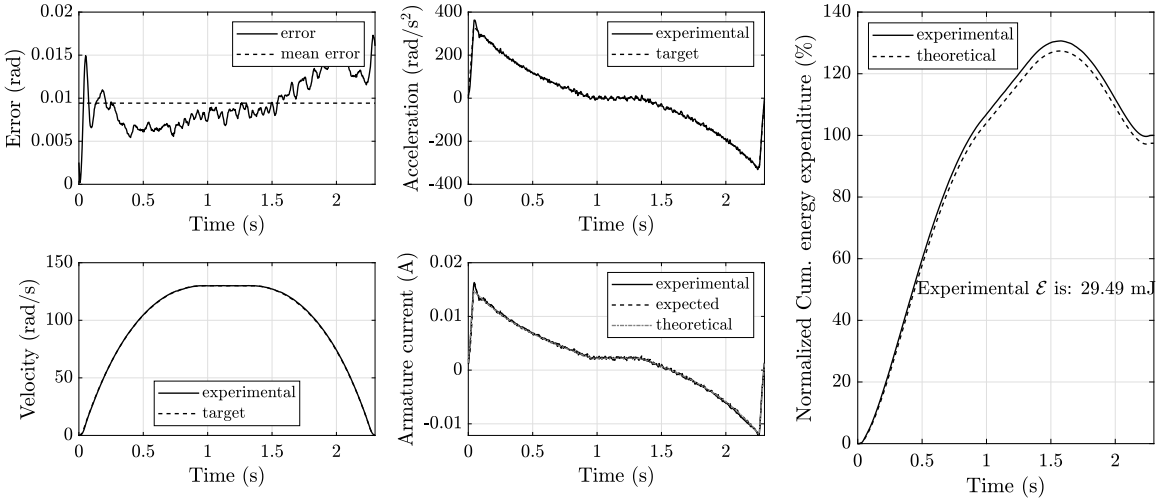

Fig. 11. Test # 2: regeneration with velocity limit.

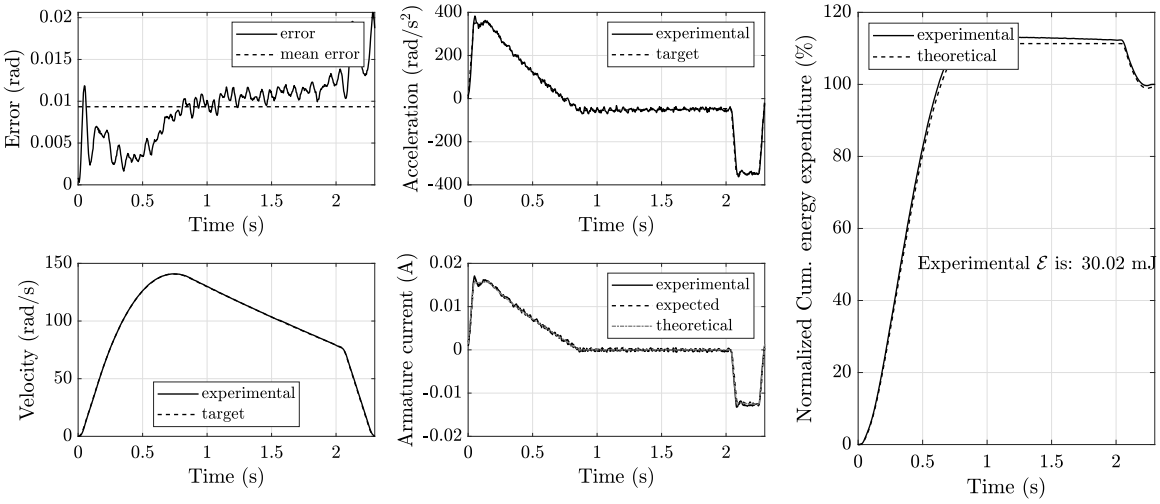

Fig. 12. Test # 3: dissipation without velocity limit.

function. The method is developed using variational calculus by exploiting the analytic representation of the optimal motion profile as a set of sequential phases, allowing to translate the motion optimization procedure into a problem formulated by a set of either linear or nonlinear equations, which are, if needed, augmented with a basic optimization problem. The solution is found by collecting pieces of

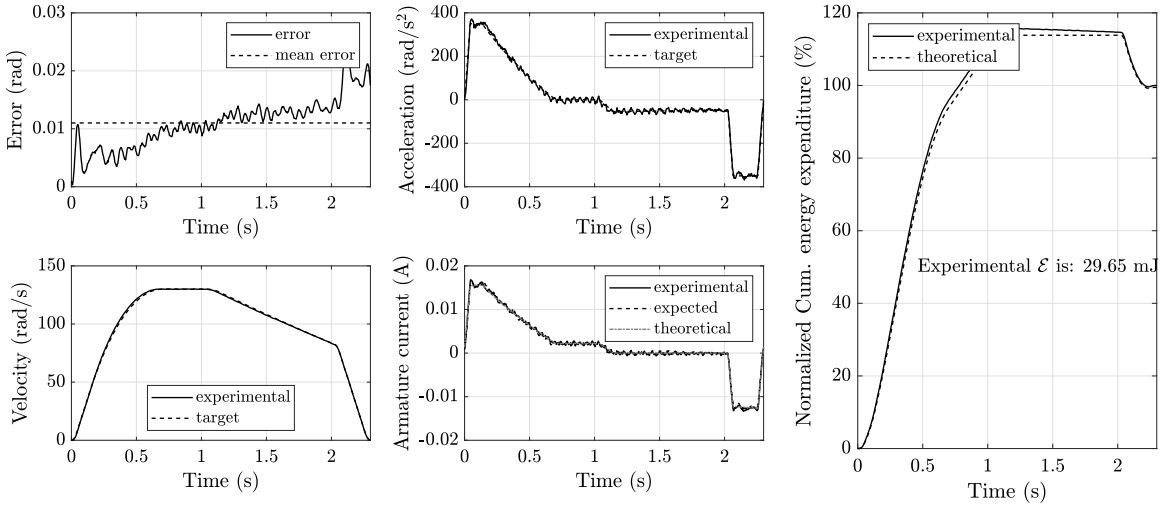

Fig. 13. Test # 4: dissipation with velocity limit.

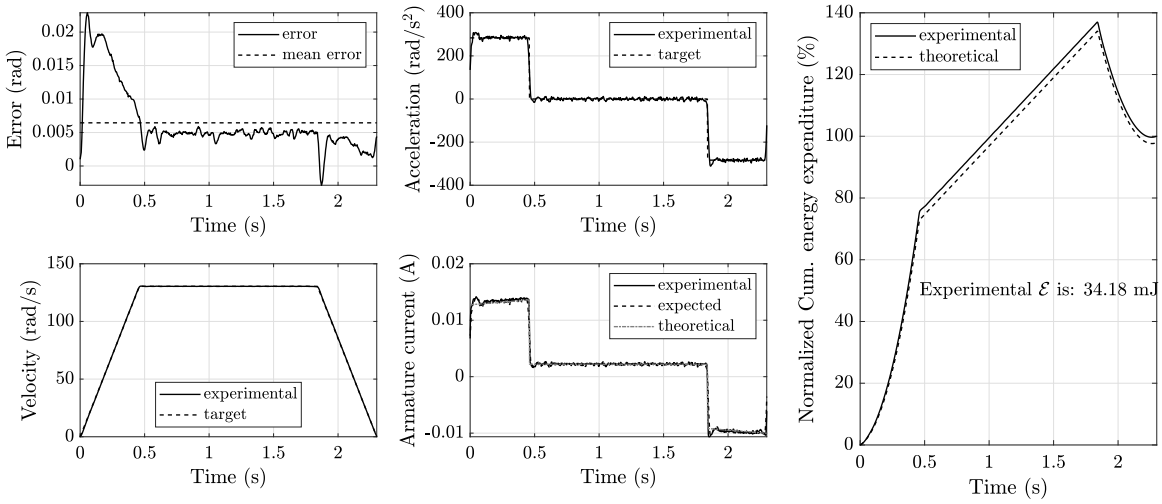

Fig. 14. Test # 5: reference symmetrical trapezoidal law.

the trajectory using BCs, instead of using direct or indirect methods. Simulation results demonstrated that the algorithm takes from roughly 1.7 to 47 milliseconds to find the solution, making it suitable for Real-Time applications. The accuracy of the solutions is shown by the comparison with the solutions obtained using a general-purpose optimal control solver, which however takes sensibly larger solution times and is totally unfit to a Real-Time application. Experimental results have been presented as well, to show that the method actually delivers the significant energy saving figures that are predicted theoretically.

Funding

This research did not receive any specific grant from funding agencies in the public, commercial, or not-for-profit sectors.

Declaration of competing interest

The authors declare that they have no known competing financial interests or personal relationships that could have appeared to influence the work reported in this paper.

References

Assad, F., Rushforth, E., Ahmad, B., Harrison, R., et al. (2018). An approach of optimising S-curve trajectory for a better energy consumption. In *2018 IEEE 14th international conference on automation science and engineering* (pp. 98–103). IEEE.

Bettega, J., Richiedei, D., Tamellin, I., & Trevisani, A. (2023). Reducing energy consumption and driving torque in an underactuated robotic arm through natural motion. In *International workshop IFToMM for sustainable development goals* (pp. 89–96). Springer.

Biagiotti, L., & Melchiorri, C. (2008). *Trajectory Planning for Automatic Machines and Robots*. Springer Science & Business Media.

Bryson, A. E., & Ho, Y.-C. (2018). *Applied optimal control: Optimization, estimation, and control*. Routledge.

Carabin, G., Wehrle, E., & Vidoni, R. (2017). A review on energy-saving optimization methods for robotic and automatic systems. *Robotics*, *6*(4), 39.

De Almeida, A., Fong, J., Brunner, C., Werle, R., & Van Werkhoven, M. (2019). New technology trends and policy needs in energy efficient motor systems-A major opportunity for energy and carbon savings. *Renewable and Sustainable Energy Reviews*, *115*, Article 109384.

Du, C., Plummer, A., & Johnston, D. (2017). Performance analysis of a new energy-efficient variable supply pressure electro-hydraulic motion control method. *Control Engineering Practice*, *60*, 87–98. http://dx.doi.org/10.1016/j.conengprac.2017.01.002.

Engelmann, J. (2009). *Methoden Und Werkzeuge Zur Planung Und Gestaltung Energieeffizienter Fabriken*. IBF.

Hagn, U., Nickl, M., Jörg, S., Passig, G., Bahls, T., Nothhelfer, A., et al. (2008). The DLR MIRO: a versatile lightweight robot for surgical applications. *Industrial Robot: An International Journal*.

Ho, T., Suzuki, K., Tsume, M., Tasaki, R., Miyoshi, T., & Terashima, K. (2019). A switched optimal control approach to reduce transferring time, energy consumption, and residual vibration of payload's skew rotation in crane systems. *Control Engineering Practice*, *84*, 247–260. http://dx.doi.org/10.1016/j.conengprac.2018.11.018.

Huang, M.-S., Hsu, Y.-L., & Fung, R.-F. (2011). Minimum-energy point-to-point trajectory planning for a motor-toggle servomechanism. *IEEE/ASME Transactions on Mechatronics*, *17*(2), 337–344.

Kim, Y.-J. (2015). Design of low inertia manipulator with high stiffness and strength using tension amplifying mechanisms. In *2015 IEEE/RSJ international conference on intelligent robots and systems* (pp. 5850–5856). IEEE.

Kim, C. H., & Kim, B. K. (2007). Minimum-energy translational trajectory generation for differential-driven wheeled mobile robots. *Journal of Intelligent and Robotic Systems*, *49*, 367–383.

Kim, H., & Kim, B. K. (2013). Online minimum-energy trajectory planning and control on a straight-line path for three-wheeled omnidirectional mobile robots. *IEEE Transactions on Industrial Electronics*, *61*(9), 4771–4779.

Lin, X., Liang, Z., Shen, L., Zhao, F., Liu, X., Sun, P., et al. (2023). Reinforcement learning method for the multi-objective speed trajectory optimization of a freight train. *Control Engineering Practice*, *138*, Article 105605. http://dx.doi.org/10.1016/j.conengprac.2023.105605.

Martins, F., Felgueiras, C., & Smitková, M. (2018). Fossil fuel energy consumption in European countries. *Energy Procedia*, *153*, 107–111.

Meike, D., & Ribickis, L. (2011). Recuperated energy savings potential and approaches in industrial robotics. In *2011 IEEE international conference on automation science and engineering* (pp. 299–303). IEEE.

Nie, Y., Faqir, O., & Kerrigan, E. C. (2018). ICLOCS2: Try this optimal control problem solver before you try the rest. In *2018 UKACC 12th international conference on control* (pp. 336–336).

Palomba, I., Wehrle, E., Carabin, G., & Vidoni, R. (2020). Minimization of the energy consumption in industrial robots through regenerative drives and optimally designed compliant elements. *Applied Sciences*, *10*(21), 7475.

Park, J. (1996). Motion profile planning of repetitive point-to-point control for maximum energy conversion efficiency under acceleration conditions. *Mechatronics*, *6*(6), 649–663.

Richiedei, D., & Trevisani, A. (2016). Analytical computation of the energy-efficient optimal planning in rest-to-rest motion of constant inertia systems. *Mechatronics*, *39*, 147–159.

Richiedei, D., & Trevisani, A. (2020). Optimization of the energy consumption through spring balancing of servo-actuated mechanisms. *Journal of Mechanical Design*, *142*(1), Article 012301.

Saidur, R. (2010). A review on electrical motors energy use and energy savings. *Renewable and Sustainable Energy Reviews*, *14*(3), 877–898.

Scalera, L., Carabin, G., Vidoni, R., & Wongratanaphisan, T. (2019). Energy efficiency in a 4-DOF parallel robot featuring compliant elements. *International Journal of Mechanics and Control*, *20*(02), 49–57.

Tho, H. D., Kaneshige, A., & Terashima, K. (2020). Minimum-time S-curve commands for vibration-free transportation of an overhead crane with actuator limits. *Control Engineering Practice*, *98*, Article 104390. http://dx.doi.org/10.1016/j.conengprac.2020.104390.

Wang, Y., Ueda, K., & Bortoff, S. A. (2012). On the optimal trajectory generation for servomotors: a Hamiltonian approach. In *2012 IEEE 51st IEEE conference on decision and control* (pp. 7620–7625). IEEE.

Wang, Y., Ueda, K., & Bortoff, S. A. (2013). A Hamiltonian approach to compute an energy efficient trajectory for a servomotor system. *Automatica*, *49*(12), 3550–3561.

Wang, Y., Zhao, Y., Bortoff, S. A., & Ueda, K. (2014). A real-time energy-optimal trajectory generation method for a servomotor system. *IEEE Transactions on Industrial Electronics*, *62*(2), 1175–1188.

Xu, X., & Antsaklis, P. J. (2003). Results and perspectives on computational methods for optimal control of switched systems. In *International workshop on hybrid systems: Computation and control* (pp. 540–555). Springer.

Yu, Z., Han, C., & Haihua, M. (2015). A novel approach of tuning trapezoidal velocity profile for energy saving in servomotor systems. In *2015 34th Chinese control conference* (pp. 4412–4417). IEEE.